Journal of Mechanics Engineering and Automation 2 (2012) 341-348

Design, Development and Experimental Characterization of a Force Sensor for Haptic Interfaces

Paolo Righettini, Roberto Strada, Alberto Oldani and Andrea Ginammi

Department of Design and Technologies, Faculty of Engineering, University of Bergamo, Dalmine 24044, Italy

Received: March 08, 2012 / Accepted: March 28, 2012 / Published: June 25, 2012.

Abstract: Working force measurement is a very important topic for several applications: In industrial field, it allows people to control the tools' wear and the working's quality; in robotics field, it allows people to control the force applied by the end-effector; on haptic interfaces, it allows the feedback between system and operator. This work deals with the design, development and experimental characterization of a three axis strain gauge force sensor for haptic interfaces. A constraint of the design and development process has been the integration of the sensor inside the structure of a haptic device developed in previous works. The end-effector of such haptic device has three degrees of freedom, and in particular it can accomplish only translational motions, while rotations aren't allowed. Hence the sensor must be able to measure only the three spatial components of the force acting on the end-effector itself. After the design and development phases, experimental tests have been carried out in order to characterize the sensor from both the static and the dynamic point of view.

Key words: Force sensor, haptic interfaces, experimental tests, static characterization, dynamic characterization.

1. Introduction

Working force measurement is a very important topic for several applications: In industrial field, it allows people to control the tools' wear and the working's quality; in robotics field, it allows people to control the force applied by the end-effector; in haptic interfaces field, it allows the feedback between system and operator.

This work deals with the design development and experimental characterization of a three axis strain gauge force sensor for haptic interfaces (Fig. 1). The design and development of the sensor have been carried out with the aim of integrating the sensor itself inside the structure of a haptic device developed in previous works.

In particular, the sensor must be housed in the device's end-effector in order to directly measure the force between the operator's hand and the haptic device, allowing a direct feed-back of the force perceived by the operator. The end-effector of such haptic device has three degrees of freedom, and in particular it can accomplish only translational motions, while rotations aren't allowed. Hence, the sensor must be able to measure only the three components of the force acting on the end-effector. The authors decided to design and develop by themselves the sensor, rather than to choose it from the market, mainly for the following reasons: It is much more cost effective; it allows full integration in the haptic device previously developed; it allows the authors to gain a higher level of customization. In

Paolo Righettini, associate professor, research fields: mechatronic systems, kinematic and dynamic of redundant robots, automatic machines, multi-body systems, real-time systems, automatic control, electric actuators, pneumatic actuators, piezo-electric actuators, active vibration control.

Alberto Oldani, research assistant, research fields: mechatronic systems, kinematic and dynamic of vehicles, multi-body systems, real-time systems, HIL systems, automatic control.

Andrea Ginammi, research assistant, research fields: mechatronic systems, multi-body systems, kinematics and dynamics of parallel kinematic robots, haptic interfaces.

Corresponding author: Roberto Strada, assistant professor, research fields: mechatronic systems, electric actuators, modeling and simulation of fluid power systems and components (pneumatics, hydraulics), active vibration control. E-mail: roberto.strada@unibg.it.

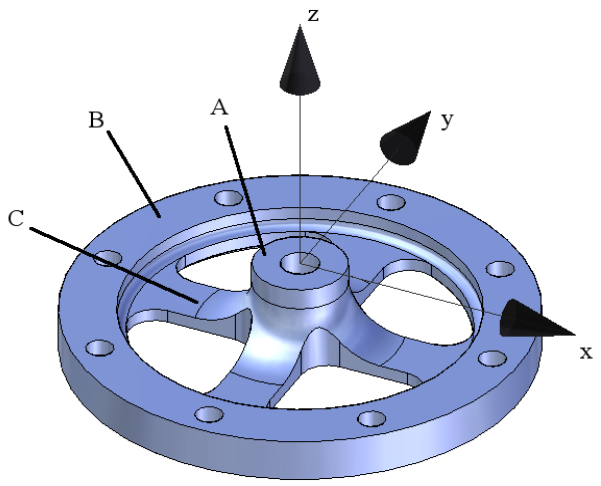

Fig. 1 3D model of the force sensor.

particular, the sensor is equipped only with the electronics for the signal amplification, while the signal processing is left to the data acquisition system that will be used.

Experimental tests have been carried-out according to the recommendations of the standards about the measurements and the methodologies for the characterization of measurement instruments [1]. The paper ends with the report of the results of the measurements carried-out.

The paper is organized as follows: In section 2, both analytical and numerical sensor's design process is outlined; section 3 describes the strain gauges configuration and the relevant signal conditioning circuit; in section 4, the strain gauges' signal composition is described; section 5 reports both the static and dynamic tests carried-out; section 6 highlights some remarks and conclusions.

2. The Design Process

As already mentioned, target of the force sensor is to measure the three spatial components of a force applied to the end-effector of a haptic interface developed within previous activities.

In order to be suitable for the haptic application, the sensor must guarantee a good quality of the output signal even when it works in the lower part of the measurement range. Moreover, its frequency response function should be constant up to 80 Hz.

From a static point of view, the design specification is an 80 N force.

The need to have a good measure also around zero (very low or no force applied) states a design's guideline: The structure of the sensor must be clearance-free, hence all its constituent elements must be rigidly coupled. Starting from the available literatures Refs. [2-9], a monolithic structure has been chosen (Fig. 1).

As Fig. 1 shows, the sensor has an inner rigid part (A) connected to an outer rigid ring (B) by means of four deformable elements (C), where strain gauges are applied (Fig. 2).

The device's symmetry with respect to z axis guarantees a response uniformity along axes x and y; as far as the forces acting along z are concerned, they result in bending of all the four deformable elements.

As regards the material type, it is an aluminium alloy with the following characteristics:

- Young modulus E = 72,600 N/mm^2;
- Yield strength σ_y = 140 N/mm^2;
- Admissible stress σ_{adm} = 170 N/mm^2.

2.1 Analytical Modeling

As first design step, an analytical model has been set-up; a single deformable element of the sensor is taken into consideration on which a generic force, represented by its components, is applied. The deformable element is considered as a cantilever with a width of 6 mm and a longitudinal section equal to the sensor's cross section, being the fixed-end the sensor's inner part, and the free-end the outer ring. The vertical force is considered equally divided on four deformable elements, while the horizontal one is considered divided on two opposite elements (e.g., 1 and 3 in Fig. 2), neglecting torsion on the other two elements (2 and 4 in Fig. 2). Hence, with reference to Fig. 3 where the sketches of the deformable elements modelled as cantilever beams are shown, the applied total force F_T and the components F_X and F_Z are related as follows:

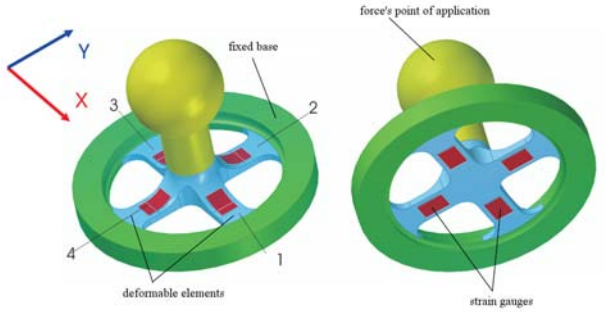

Fig. 2 Strain gauges position.

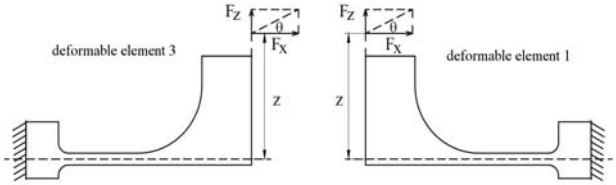

Fig. 3 Cantilever sketch of the deformable elements.

$$F_X = \frac{F_T}{2}$$
$$F_Z = \frac{F_T}{4} \quad (1)$$

In particular, the design force is an 80 *N* force lying on the *xz* plane with angle $\theta = 45°$ and applied on the upper surface of the sensor's inner part ($z = 9.5$ mm).

Two opposite deformable elements are considered, e.g., with reference to Fig. 2, elements 1 and 3. In this way, both compressive and tensile actions of the applied force are taken into consideration.

The goal of the analysis is to define a geometry (with particular reference to the thickness of the deformable elements) such that a deformation $\epsilon \geq 1{,}300$ με on the deformable elements can be obtained.

Fig. 4 depicts the deformation for the upper and lower sides of the two deformable elements for 1 mm thickness. As it can be noted in the graphs, in all the four cases, there are zones where the deformation is higher or around 1,300 με. Hence, the best zone applying the strain gauges seems to be the one near to the inner fillet.

2.2 Finite Element Model

Because of the simplifications of the analytical model, a more accurate model is needed in order to validate the results previously obtained.

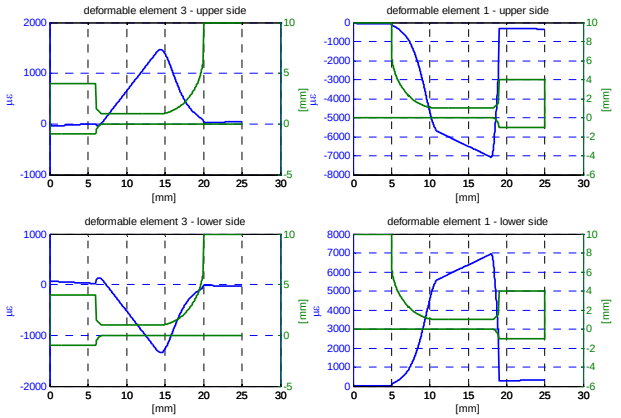

Fig. 4 Analytical model results.

With this aim, a finite element analysis has been performed by means of commercial software: MD.Nastran as solver and MD.Patran as pre- and post-processor. Fig. 5 shows the finite element model of the sensor; the simulation has been carried out only on the sensor, without modelling the knob for the interaction with the outside world. Moreover, as for the analytical model, an 80 N load has been applied at the upper surface of the sensor's inner part.

The load in the Finite Element Method (FEM) model has been applied by means of rigid elements connecting the sensor's upper face and the force's point of application (Fig. 6).

This way of load application allows uniformly distributing the load on the upper surface. As regards the constraints, the nodes of the upper and lower surface of the external ring are fixed.

Fig. 7 depicts the results of the FEM analysis in terms of Von Mises strains, along with the magnified deformation of the system. The label shows that the maximum strain is around 1,300 με, as the design target is. The graphs in Fig. 8 are the behaviour of the strains' components along the path highlighted in Fig. 5. The red line graph concerns the upper side, while the green one concerns the lower side. It should be noted that the strains on the deformable elements are slightly different from the ones derived from the analytical model, mainly as regards the strains on the deformable element 1 (the right side of the graphs). It is clear that, because of the simplification of the analytical model, it

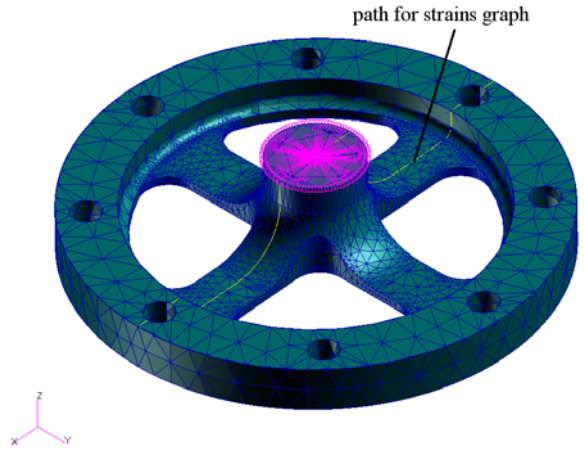

Fig. 5 Finite element model.

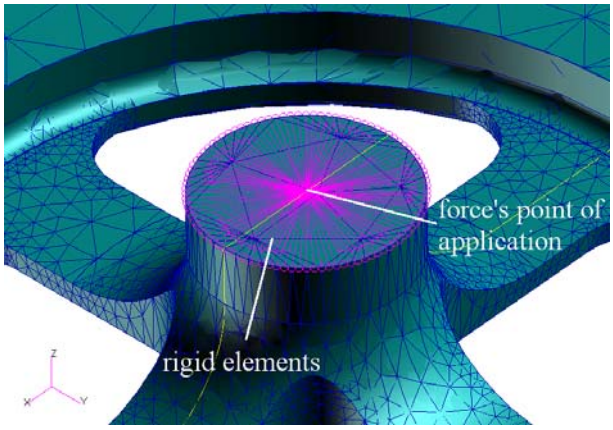

Fig. 6 Detail of the rigid elements for load application.

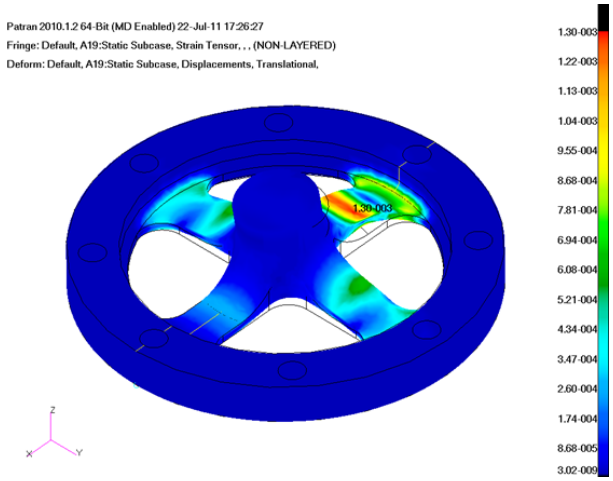

Fig. 7 Results of the FEM analysis.

overestimates the strains in element 1, while the results of the two models are more similar with element 3.

However, the FEM model confirms that with 1 mm thickness, there are zones on the elements exceeding 1,300 με.

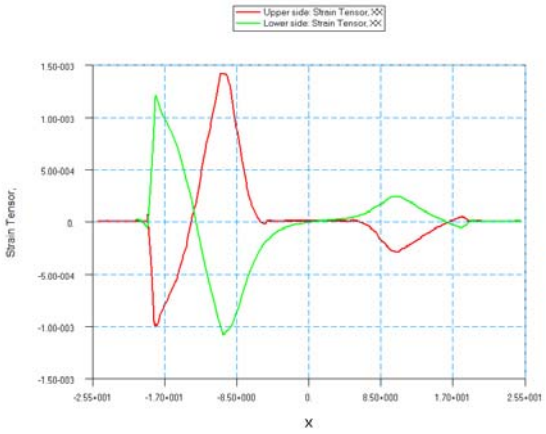

Fig. 8 Strains along the deformable elements.

2.3 Strain Gauges Positioning

In order to maximize the electrical signal from the strain gauges, they have been placed around the zone of maximum strain. From Fig. 8, it's clear that the best zone is around the inner fillet, as obtained from the analytical model. Moreover, the mean value of the strains on a 3 mm × 3 mm square has been calculated; Fig. 9 shows the results.

Looking at the graph of Fig. 9, it's clear that the most appropriate zone where to place the strain gauges is the one between 8.5 mm and 11.5 mm from the sensor's centre. On this length, where the mean strains for the upper side is 1,355 με, the strain gauge's sensing zone will be placed. As far as the lower side is concerned, the position where the means strain is maximum is the same and the relevant value is 1,274 με.

3. Electronic Circuit

As shown in Fig. 10, two strain gauges on each deformable element have been placed, one on the upper side and the other on the lower side; this choice allows compensating for thermal expansions. As a matter of fact, by connecting the strain gauges on two adjoining arms of the Wheatstone bridge, their signals subtract each other, hence the apparent strains due to thermal expansion results in a null signal. On the contrary, the signals due to the applied force, that acts as a bending moment on the deformable elements, are of opposite sign, hence they sum each other [10-11].

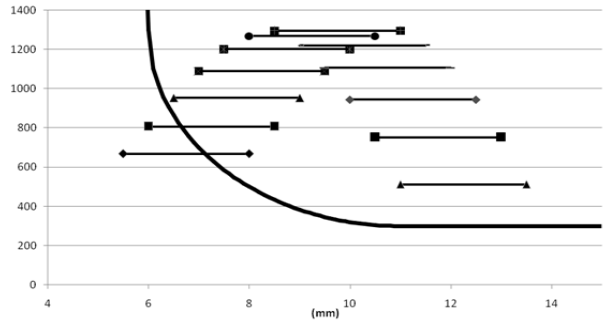

Fig. 9 Strains mean values for the upper side results of the FEM analysis.

Fig. 10 The force sensor realized, with the relevant strain gauges.

Moreover, the half bridge configuration adopted allows compensating for the torsional effects on the other two elements, e.g., the strains arising on elements along Y direction due to the force acting along X direction.

The signal conditioning circuit is composed by four stages, one for each Wheatstone bridge. Each stage has a trimmer for the bridge balancing, an instrumentation amplifier to amplify the bridge signal and two resistors (the other half of the bridge).

The circuit has been realized on a very small board in order to be housed in the haptic interface's end-effector. Fig. 11 shows the sensor's housing: knob (1), covering plate (2), force sensor (3), electronic circuit (4), end-effector (5).

4. Signals Composition

Let's note that force's components along *x* axis and along *y* axis cause strains of different sign in the two involved deformable elements. So, in order to get the force's component, the two signals must be subtracted. In particular, if *out1* and *out3* are the signals coming from the strain gauges placed on element 1 and element 3 (Fig. 2), the force is

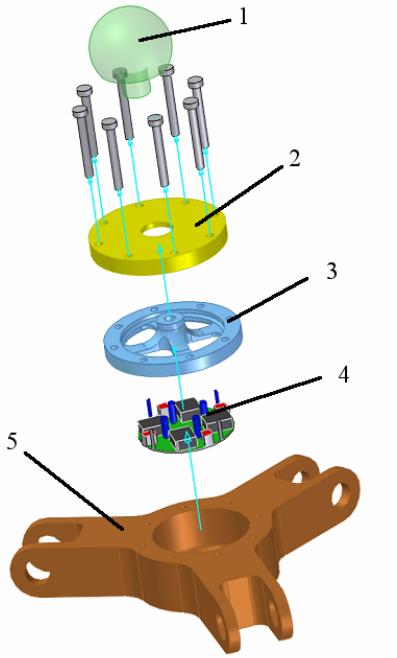

Fig. 11 Sensor's housing.

$$outF_x = \frac{out1 - out3}{2} \tag{2}$$

where $outF_x$ is signal in Volts; in the next section the static experimental tests to define the calibration curves of the sensor.

Similarly, for the *y* force's component:

$$outF_y = \frac{out2 - out4}{2} \tag{3}$$

As far as the *z* component is concerned, four nominally equal signals are obtained; hence,

$$outF_z = \frac{out1 + out2 + out3 + out4}{4} \tag{4}$$

5. Experimental Tests

In this section, the results of either the static or the dynamic experimental tests are reported.

5.1 Static Experimental Tests

The tests have been carried-on applying to the sensor some calibrated known weights along different directions. Tests are of two main types:

- Along the main axes *x*, *y* and *z*;
- Along directions lying in a plane defined by two main axis.

Fig. 12 shows the result of the test concerning loads

applied along the positive X direction. The figure depicts the signals of channels 1 and 3 (signals from the strain gauges of deformable elements 1 and 3) showing a very good linearity. The signals of channels 2 and 4 show the absence of cross-talking effects. Fig. 13 shows the results of an analogous measure carried on by applying a force along the positive direction of axis *z*. Also in this case, all the four channels show a very good linearity. Figs. 14-15 depict the behaviour of the angle and force's module estimation error for different angles of a force lying in *xy* plane. Similarly, Figs. 16-17 show the errors for different angles of a force lying in *xz* plane.

5.2 Dynamic Experimental Tests

The dynamic tests have been carried on by applying a variable frequency harmonic force to the sensor with the aim of investigating the frequency response of the sensor itself. In particular, the sensor has been rigidly connected to a fixed base and a harmonic force along –Y direction has been applied by means of a shaker. The

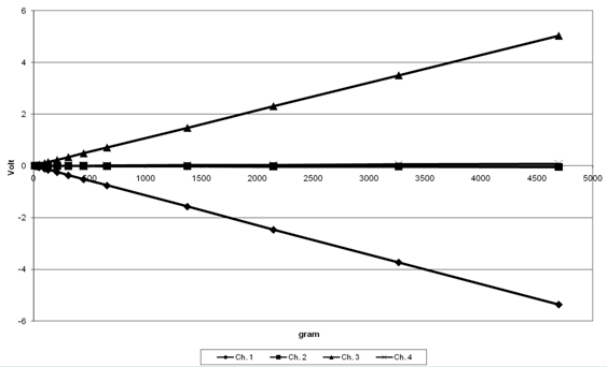

Fig. 12 Load test in +X direction.

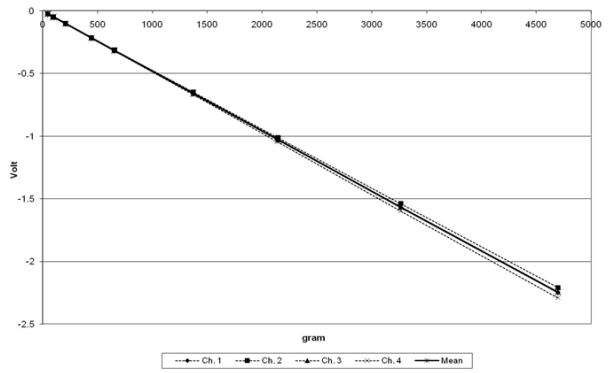

Fig. 13 Load test in +Z direction.

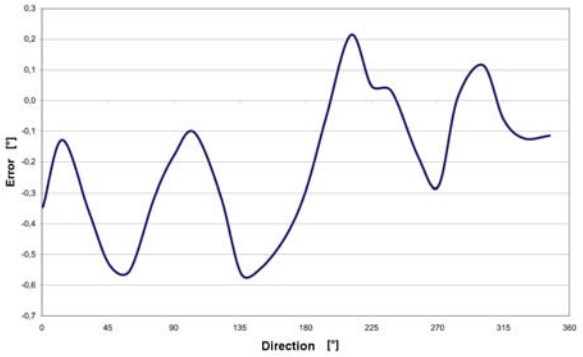

Fig. 14 Angle detection error in *xy* plane.

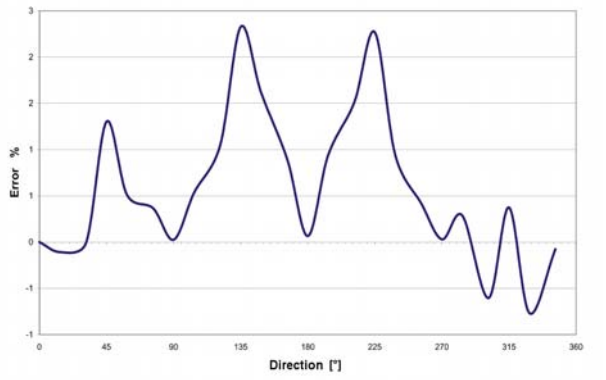

Fig. 15 Force's module error vs. angle in *xy* plane.

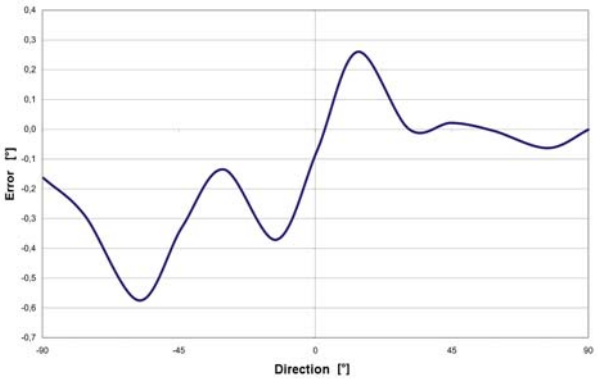

Fig. 16 Angle detection error in *xz* plane.

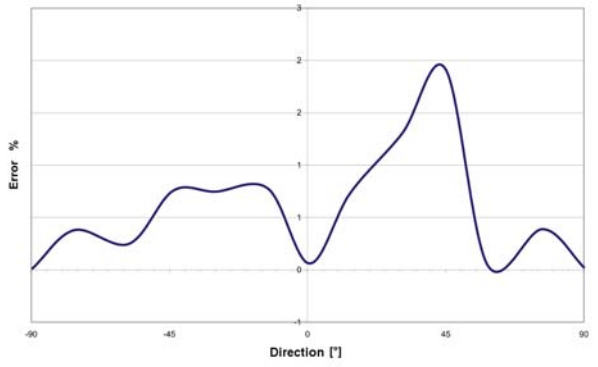

Fig. 17 Force's module error vs. angle in *xz* plane.

shaker has been driven with a sine sweep; this kind of signal has allowed investigating the dynamic behaviour of the sensor inside the frequency range of interest (as already mentioned, up to 80 Hz). Fig. 18 shows the experimental set-up, while Fig. 19 shows the relevant results.

As shown in Fig. 19, experimental tests highlighted a frequency range where the frequency response is constant and unitary. It should be noted that the frequencies of interest (up to 80 Hz) are inside the highlighted range.

6. Conclusions

This work deals with the design and development of a strain gauge force sensor for a haptic interface device. The main design guidelines have been the absence of clearance in the sensors structure and small dimensions in order to be housed, along with its electronic circuit for signal conditioning, in the end-effector of the haptic interface. So a monolithic small structure has been realized.

The design has been carried on both by an analytical approach and a finite element analysis.

The tests have given good results: The sensor has good linearity and gives good quality signals. Furthermore, the angle detection and force's module error are small and very suitable for the application.

As far as dynamic tests are concerned, only a test has been carried on by applying a variable frequency force along –Y direction. These tests have shown a constant and unitary frequency response for the frequency range of interest.

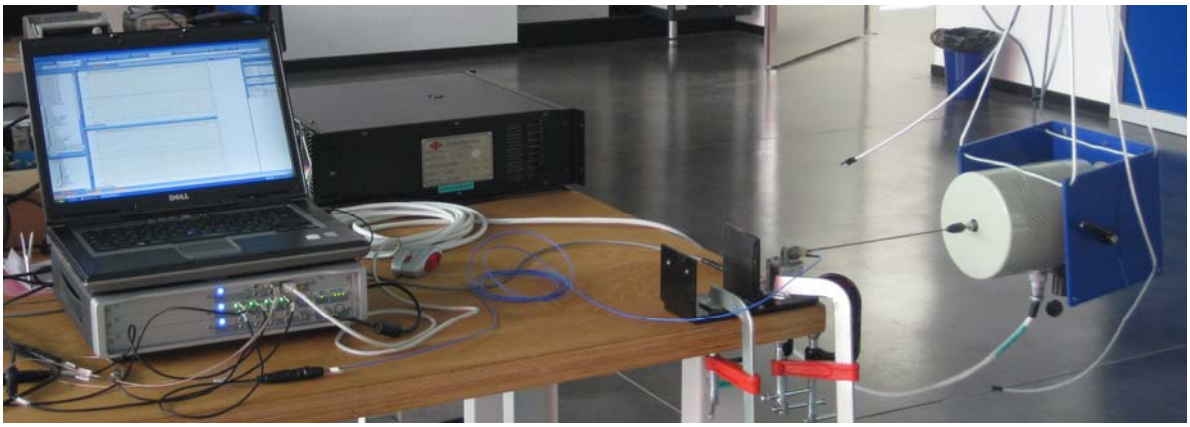

Fig. 18 Experimental set-up.

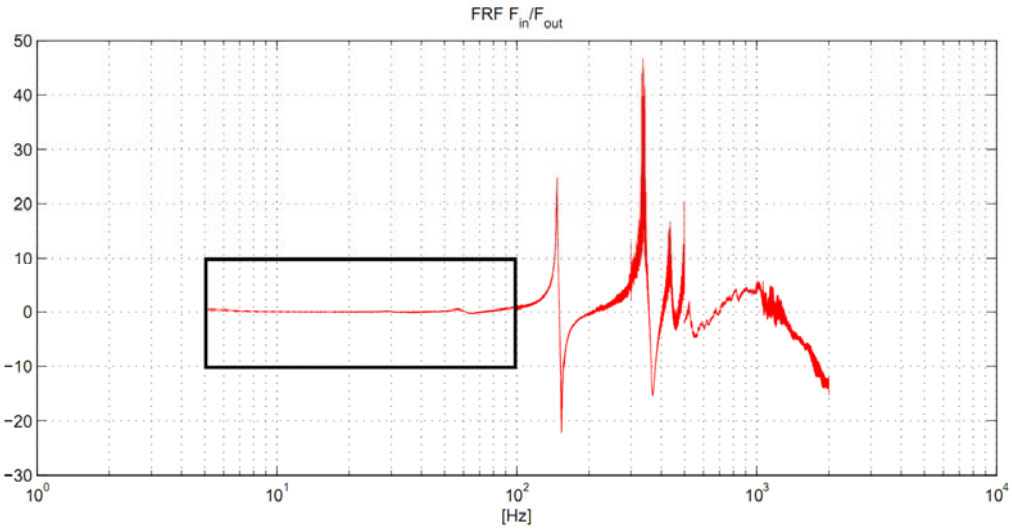

Fig. 19 Measured FRF.

Future works will deal with other dynamic tests in order to fully characterize the sensor from the dynamic point of view. In particular the behaviour beyond 80-100 Hz will be investigated in details.

References

[1] International Standard—UNI ISO 5725.

[2] M.M. Svinin, M. Uchiyama, Optimal geometric structures of force/torque sensor, The International Journal of Robotics Research 14 (6) (1995) 560-573.

[3] A. Lorenz, M.A. Peshkin, J.E. Colgate, Force sensor for human robotics interaction, in: 1999 International Conference on Robotics and Automation, Detroit, MI, 1999.

[4] P. Righettini, H. Giberti, G. Olgiati, R. Strada, Design of a sensorised end-effector for robotic tooling operations, International Journal of Mechanics and Control 4 (2003) 21-26.

[5] G.S. Kim, Development of a three-axis gripper force sensor and the intelligent gripper using it, Sensors and Actuators A: Physical 137 (2) (2007) 213-222.

[6] T. Endo, H. Kawasaki, K. Kouketsu, T. Mouri, High-precision three-axis force sensor for five-fingered haptic interface, in: J.G. Rocha, S. Lanceros-Mendez (Eds.), Sensors, Focus on Tactile, Force and Stress Sensors, I-Tech, Vienna, Austria, 2008, pp. 87-102.

[7] M. Sorli, S. Pastorelli, Six-axis Reticulated Structure Force/Torque Sensor with Adaptable Performance, Elsevier, 1995.

[8] L.P. Chao, K.T. Chen, Shape Optimal Design and Force Sensitivity Evaluation of Six-Axis Force, Elsevier, 1996.

[9] G.S. Kim, The design of a six-component force/moment sensor and evaluation of its uncertainty, Measurement Science Technology 12 (2001) 1445-1455.

[10] E.O. Doebelin, Measurement Systems: Application and Design, McGraw-Hill, 2004.

[11] A. Cigada, L. Comolli, S. Manzoni, Estensimetria Elettrica, CittàStudi Edizioni, 2008.